universe

MDPI

Article

More Efficient and Reliable: Identifying RRab Stars with Blazhko Effect by Deep Convolutional Neural Network

Nan Jiang [1,2], Tianrui Sun [3,4], Siyuan Pan [5], Lingzhi Wang [6,7], Xue Li [2], Bin Sheng [5] and Xiaofeng Wang [2,*]

1 David A. Dunlap Department of Astronomy and Astrophysics, University of Toronto, 50 St. George Street, Toronto, ON M5S 3H4, Canada
2 Tsinghua Center for Astrophysics, Physics Department, Tsinghua University, Beijing 100084, China
3 Purple Mountain Observatory, CAS, No. 10 Yuanhua Road, Qixia District, Nanjing 210023, China
4 School of Astronomy and Space Sciences, University of Science and Technology of China, 96 Jinzhai RD, Hefei 230026, China
5 Department of Computer Science and Engineering, Shanghai Jiao Tong University, Shanghai 200240, China
6 Chinese Academy of Sciences, South America Center for Astronomy (CASSACA), National Astronomical Observatories, CAS, Beijing 100101, China
7 CAS Key Laboratory of Optical Astronomy, National Astronomical Observatories, Chinese Academy of Sciences, Beijing 100101, China
* Correspondence: wang_xf@mail.tsinghua.edu.cn

Abstract: The physical origin of the Blazhko effect (BL), a phenomenon of a single or multiple periodic modulation(s) of the light curve, is under debate. Efficiently identifying and characterizing the BL is essential in understanding its origins and accounting for its effect on numerous applications of RRabs in the era of large time-domain surveys. In this study, we make use of Resnet 34, a well-known convolutional neural network (CNN) architecture, to identify RRab stars with BL from phased light curves collected from OGLE. Using reliably classified RRabs from frequency analysis to train, validate, and test our model, we show that our CNN method reaches accuracies up to 94%. We then applied our CNN method to some additional RRabs located in the Magellanic Cloud (MC) and the Galactic Bulge (GB), leading to the discovery of 113 and 2496 BL candidates, respectively. The identification accuracy for the MC Sample is estimated to be 91% after cross-matching the CNN classification results with those from frequency analysis. Similarly, the light-curve parameters of these classified BL/non-BL candidates by our CNN method from the GB region resemble those observed in the literature, confirming the reliability of our CNN classifications. Our CNN method is subject to issues related to light-curve quality and sampling, but its overall reliance on light-curve quality is comparable to that of frequency analysis. Furthermore, we find that BL modulation could be primarily characterized by variations in light-curve structure.

Keywords: stars: variables; RR Lyrae methods; data analysis techniques; photometric

Academic Editor: Denis Leahy

Received: 31 October 2024
Revised: 27 December 2024
Accepted: 30 December 2024
Published: 6 January 2025

Citation: Jiang, N.; Sun, T.; Pan, S.; Wang, L.; Li, X.; Sheng, B.; Wang, X. More Efficient and Reliable: Identifying RRab Stars with Blazhko Effect by Deep Convolutional Neural Network. *Universe* **2025**, *11*, 13. https://doi.org/10.3390/universe11010013

1. Introduction

RR Lyrae stars (RRLs) are relatively old and low-mass stars that show regular light variations. Most of their periods and amplitudes vary in the range from 0.2 to 1 day [1] and 0.2 to 2.0 mag in the *V* band [2], respectively. RRLs can be roughly classified into three main subclasses based on the shapes of their light curves [1]: RRab (rapid increase followed by slow decrease), RRc (similar to sine curve), and RRd (double-mode pulsating). RRLs have been applied well to study various aspects of astrophysics. To begin with, RRLs can be used as standard candles. For instance, Oliveira et al. [3] made use of the

Period–Luminosity–Metallicity relation for RRL stars to estimate distances to six globular clusters. RRLs have also been used to map galactic structure [4].

Because of their many useful applications, RRLs have been intensively identified and studied in various large time-domain surveys. The analysis of observation data from the Massive Compact Halo Objects project [5] led to the discovery of ∼10,000 RR Lyrae stars from monitoring the fields of Magellanic Clouds (MC), the Galactic Bulge (GB), and the Sgr dwarf galaxy. In the observations of the past two decades, the Optical Gravitational Lensing Experiment project (OGLE, [6–8]) discovered 126,146 RRLs stars in total from the Galactic Disc/Gulge and MC sky areas. Numerous RR Lyrae stars have also been extensively discovered during surveys such as the Catalina sky survey [9], ASAS [10], Pan-STARRS1 [11], and LINEAR [12]. More recently, Gaia has identified a total of 271,779 RRLs from the whole sky during data release 3 (GDR3, [13]). More RR Lyrae stars are expected to be identified by the Legacy Survey of Space and Time (LSST, [14]).

Some RRab stars are known to display the Blazhko (BL) effect, characterized by modulations in their periods, pulsation amplitudes, light-curve shapes, and radial velocities [15,16]. Many interesting characteristics of BL stars have been revealed in the literature, for example, high incidence rate [17], high modulation [18], high likelihood of strongly asymmetric sidelobes in the frequency spectra [19], large range of modulation timescales [20], period-doubling [21], and chaotic/stochastic effects [22]. BL stars usually show light variations, with amplitude ranging from a few hundredths of magnitude (e.g., 0.015 mag for KIC 11125706 [23]) to more than 0.5 mag (e.g., XY Eri or SZ Hya [24]). Such light-curve variations can be also identified through an analysis of frequency spectra [25–27].

Despite many light-curve features that have been revealed for BL stars, their physical origins remain unknown. Nevertheless, these light-curve characteristics could provide insights into the modulation mechanisms and impose additional constraints on existing models. Studies by Gillet [28] and Gillet and Fokin [29] proposed that the BL effect might be induced by the shockwave phenomenon based on spectroscopic observations of some BL stars. They proposed that the existence of a secondary shock could lead to modulations of the light curves. Recent studies by Jurcsik et al. [30,31] found that BL stars showed limited modulations in near-infrared bands and that the light-curve modulations tend to depend on the modulated temperature. This provides evidence that the BL effect is related to the outer layers of the stars. After evaluating the existing models, Kolláth [32] concluded that Buchler and Kolláth [16]'s fundamental to 9th overtone, or 9:2 resonance hypothesis, shows the fewest conflicts with the observations.

BL stars are commonly identified through their distinct characteristics of frequency spectra. The frequency spectra of BL stars are characterized by equidistant side peaks, i.e., f_{BL} around the fundamental pulsation frequency (dubbed as f_0). Meanwhile, if the BL star also shows amplitude modulation, then f_{BL} could appear on its own in the range of ∼0.0001 to 0.2 [c/d][1] [33,34]. Normally, BL samples can be identified by first estimating the basic pulsation frequency (f_0) and then searching for side peaks in the residual frequency spectrum after pre-whitening f_0. RRab stars can be identified as a BL subclass if the side peaks of their light curves have a significant signal-to-noise ratio (S/N). Several studies have adopted different definitions of significance, perhaps depending on their light curves' quality for identification [25–27,35].

With the increase in the total number of RRLs identified in recent surveys, large population studies on the characteristics of BL stars now become feasible. More importantly, such studies could act as a guide for understanding the origin of BL effects theoretically. However, since manual inspection is required throughout the classification process, it is extremely time-consuming to identify the RRLs with BL effects from a large sample using frequency analysis [25–27]. Hence, we propose to use the deep learning method to improve

the efficiency of identifying RRLs with the BL effect. We adopt a convolutional neural network (CNN): a deep learning algorithm that has been mainly used for analysis tasks such as classification, segmentation, and detection [36]. CNNs have been successfully employed in many astronomical applications, such as the classification of stellar spectra [37], detection of solar flares [38], etc.

Moreover, the CNN method has also been widely applied to detect variables or transients. For example, Mahabal et al. [39] applied this method to classify variable stars based on their light curves, while studies such as Teachey and Kipping [40] applied a CNN to identify pro-moon objects. Davies et al. [41] used this method to identify gravitational lensing events. This method has been also used to identify exoplanets from the TESS data with great performance [42,43]. Notably, refs. [44,45] make use of CNNs to classify different types of variable stars based on OGLE data and achieved good results.

In this study, we make use of the identification results proposed by Prudil and Skarka [26] (hereafter, PS17) on samples collected from the GB region and folded OGLE light curves to train our model. This CNN model is then applied to additional sets of GB and MC Samples to test the performance of the model. More specifically, frequency analysis methods used by Skarka [25], Skarka et al. [27], and PS17 [26] are applied to the new MC Sample to cross-validate the performance of the model. Given the large number of RRLs identified by OGLE, many new BL stars located in MC and GB could be classified by our model. We then examined these newly BL-classified RRL samples statistically to better understand the differences between BL and nBL stars, which could serve as clues to understanding the physical origin of the BL effect.

This paper is organized as follows. We describe the data selection process and cut-offs used for sample identification presented in Section 2. Then, in Section 3, we describe how we build, train, and test our model. We discuss the performance and limitations of our identification model in Sections 4 and 5. We summarize in Section 6.

2. Data

In this study, all of our RR Lyrae are classified by the OGLE sky survey [6–8], a long-term survey project, with the main goal of hunting for gravitational microlensing events and understanding stellar variabilities in the Milky Way, LMC, and SMC. In 2014, 2016, and 2019, the OGLE-IV survey published the V- and I-band photometric data of RR Lyrae stars discovered in the GB and MC fields, with data going back to 1996 [6–8].

We adopt the classified BL/nBL sources from PS17 [26] as our data set to train our CNN model. Given that all of these well-classified sources are located in the Galactic Bulge, we label all of them as GB Sample 1. Our GB Sample 1 (or PS17 [26] sample) consists of 3341 RRab stars with BL effects and 4845 without BL effects (nBL). To classify these sources, PS17 [26] make use of the frequency analysis method based on light curves obtained from the OGLE survey. We ignore all the samples labeled as blending by PS17 [26] for all our future analyses to avoid the impacts of these blending sources on our model. We then randomly divided the GB Sample 1 into the modeling set, the validation set, and the test set with a ratio of 7:2:1 to train, validate, and test our model for both BL and nBL samples. This ratio ensures that there is enough sample for the CNN model to learn the characteristics of BL/nBL effects while leaving a moderate amount of sample to quantify the performance of the model.

In addition, we select two groups of targets (i.e., MC Sample and GB Sample 2) from OGLE located in the Magellanic Clouds and the Bulge to further discuss the performance of our model and understand the characteristics of the BL effect. All of the sources from MC Sample data are drawn from the Magellanic Clouds. We use the MC Sample primarily

to further evaluate the performance of our model, especially on samples with degraded light curves, to identify possible biases and limitations of the model.

Meanwhile, with the release of some additional data as part of OGLE-IV [8], many targets that are not included in PS17 [26]'s analysis due to various quality cut-offs now become good enough to identify the BL effect in this study. Consequently, we constructed a new data set (i.e., GB Sample 2) based on the updated data sources to further study the characteristics of the BL effect. We would like to stress that GB Sample 1 and GB Sample 2 are purely independent, namely, none of the samples from GB Sample 1 are included in GB Sample 2.

Following PS17 [26], Skarka [25], and Skarka et al. [27], we use similar cut-offs to eliminate stars that either are too faint or contain fewer epochs per light curve. For the GB Sample 2, the selection criteria include the following:

1. The mean I-band magnitudes are smaller than 18 mags;
2. There are more than 350 data points in the light curve of each star.

These cut-offs are almost identical to the ones introduced by PS17 [26], with the exception that PS17 [26] discarded samples with fewer than 400 epochs in their study. These selection criteria yield 8123 stars for the GB Sample 2 out of the total 40,476 stars from [8]. For the MC Sample, however, we include additional selection criteria along with the above two. This is because the light curves of the stars from the MC have worse quality than the GB sample, and the photometry of some stars suffers obvious blending effects. The additional criteria are suggested by Jacyszyn-Dobrzeniecka et al. [46] and Soszyński et al. [7], as follows:

1. Mean magnitude error is smaller than 0.025 mag;
2. Amplitude of the light curve must be larger than 0.20 mag;
3. Amplitude of the light curve must be greater than $-5\log_{10}(\text{period}) - 1$.

Finally, a total of 290 out of 34,229 RRabs pass our selection criteria and can be labeled as the MC Sample. It is worth mentioning that some of our brightest stars selected for the MC Sample might be foreground. However, since the MC Sample is used to test the performance of our CNN method, we do not expect any impact on our results from these foreground stars. Also, note that only the I-band light curves are used for further evaluation because of better sampling in this band. A summary of the composition of the three groups of samples used in our analysis is shown in Figure 1. We also included the distribution of photometric errors and data sampling of the light curves for the three groups of samples in Figure 1 for further reference. Upon the visual inspection of Figure 1, we note that GB Sample 1 has significantly more data points per light curve (i.e., N = 1914) in comparison with the other two data sets, i.e., GB Sample 2 (with N = 624) and the MC Sample (with N = 471).

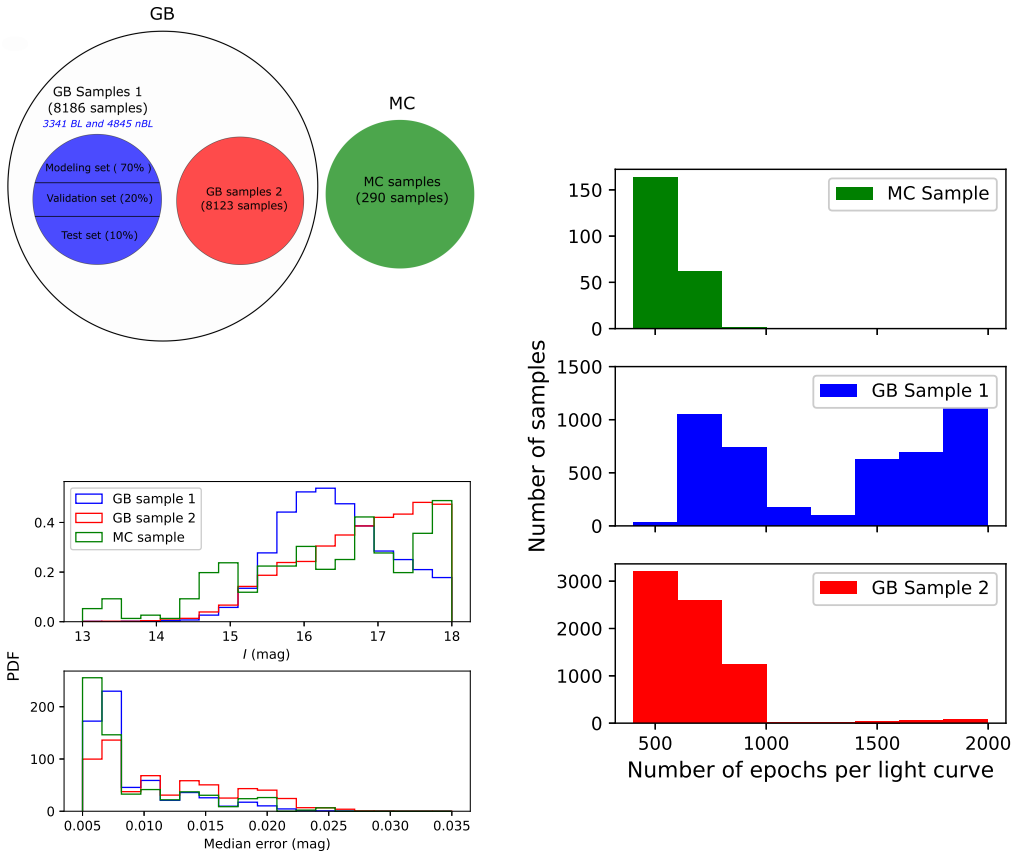

Figure 1. A summary of our selected samples used in this study. **Top Left**: a general view of the composition of the three groups of targets that we selected. **Bottom Left**: The uncertainty distribution for our sample that is brighter than 18 mag. **Right**: The number of data points in each light curve for our samples.

3. Method of Identifying BL Effect

BL effect is commonly identified through frequency analysis, but this study aimed to show that stars with the BL effect could be identified more effectively through CNN algorithms. Past studies such as Skarka [25] made use of manual procedures to hunt for BL peaks in the frequency spectra and the residuals, while, in recent years, semi-automatic procedures have been adopted by studies such as PS17 [26]. More specifically, the identification procedure from PS17 [26] involves the automatic removal of the first 10 harmonics and manual search for significant peaks near the main pulsation frequency (f_0) and $2f_0$ in the residuals using Period04 [47]. Stars with peaks having 3.5 S/N near the main pulsation frequency (f_0) and $2f_0$ are labeled as BL stars. Meanwhile, if a star shows no sign of modulation, it is labeled as nBL. However, they noted that the labeling results might be affected by different instrumental effects due to the limitations of ground-based observations.

Prudil et al. [48] (hereafter, P19) showed that the BL effect can be identified through machine learning algorithms. They quantified the performance of their classifiers by using accuracy (ACC) and area under the receiver operating curve (AUC), and their definitions can be found as follows:

1. Sensitivity/True Positive Rate (TPR): the ratio between the number predicted as positive by the classifiers and that determined based on ground truth (i.e., the frequency analysis in our context);

2. Specificity/True Negative Rate (TNR): the ratio between the number predicted as negative by the classifiers and that determined based on ground truth (i.e., the frequency analysis in our context);
3. *ACC*: the ratio between all the true values to the whole sample, and the equation can be shown below:
$$ACC = \frac{TPR + TNR}{TPR + TNR + FPR + FNR}. \quad (1)$$
TPR, TNR, FPR, and FNR denote the True Positive rate, True Negative rate, False Positive rate, and False Negative rate, respectively;
4. *AUC*: The area under the receiving operating curve (ROC). The ROC curve, standing for the receiver operating characteristic, is used to assess the performance of a binary classifier at different thresholds. Usually, AUC ranges from 0.5 to 1.0, and higher values represent better performance.

Among all the identification models developed by P19 [48], Multi-Layer Perceptron (MLP) exhibited the highest accuracy of 87.3%. MLPs, however, suffer from the issue of over-fitting due to their fully connected structure between adjacent layers, which further limits their performance during classifications. As an alternative to MLP, we propose to use the CNN algorithm, which has a more sophisticated network structure, to identify BL effects more accurately. In contrast to MLP, the CNN method is less likely to overlearn certain characteristics, making it a more reliable method for identifying BL candidates.

In general, models with more layers perform better during training since more layers allow the model to extract and combine features more effectively. In reality, as the depth of the network structure increases, if the gradients at any layer become extremely small, it becomes nearly impossible to propagate the gradients to the final layers. This results in either very slow learning or no learning at all.

Such issues are known as gradient vanishing, which have been found to limit the performance of the network during classification tasks [49]. To ensure that our network contains enough layers to fully characterize the properties of the BL effect while avoiding the issues of gradient vanishing as much as possible, we choose ResNet 34 as our classification model [50]. ResNet circumvents depth-related performance degradation through skip connections, which allow neural networks to increase the number of layers without suffering from gradient vanishing problems. ResNet-34 comprises 34 layers in total, including convolutional layers, batch normalization layers, ReLU activation functions, and max pooling layers. The ResNet architecture has been widely adopted for tasks such as image classification due to its remarkable robustness across diverse applications. It is worth mentioning that we do not make any modifications to the original ResNet 34 architecture.

Regarding the data set for the training, compared to the parametric spaces used by P19 [48], we believe that images of the phased light curves represent light curve properties better since could represent more features of BL stars compared with simple grids of light curve parameters. We present some typical phased light curves of the BL stars and nBL stars from our modelling set or PS17 [26] in Figure 2.

3.1. Network Training

3.1.1. Preprocessing

Before training the network, we apply five additional procedures to clean and normalize our data set. Firstly, we fold each light curve based on its fundamental pulsation period determined from Soszyński et al. [6–8]. We then apply a 10th-order Fourier fit to remove points that are 0.35 mag away from the best-fit light curve. The given threshold ensures scattering caused by the BL effect will not be removed, while outliers will be removed, as they might have an impact on the training.

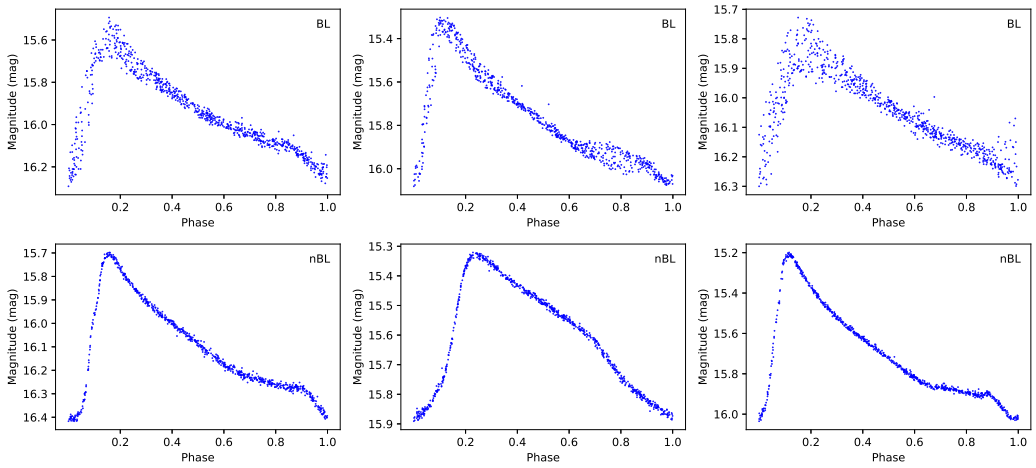

Figure 2. Top row (BL stars) from left to right: OGLE-BLG-RRLYR-00162, OGLE-BLG-RRLYR-00184, OGLE-BLG-RRLYR-00197. Bottom row (nBL stars) from left to right: OGLE-BLG-RRLYR-00183, OGLE-BLG-RRLYR-00199, and OGLE-BLG-RRLYR-00208. The period is adopted from Soszyński et al. [7]. A major distinction between BL stars and nBL sources is the large dispersion near the peak of the light curve, reflecting both the period and amplitude variation due to the BL effect.

Once this is completed, we normalize each phased light curve by subtracting the median of the light curve. We then plot the phased light curve in a frame with fixed axis coordinates. More specifically, we first plot the images in a fixed axis of $[0, 1] \times [-0.6, 0.6]$ for phase and amplitude, respectively. We then convert the output to an image using matplotlib `plt.plot` function with the total dots per inches (dpi) set to 300 and the size of each point on the plot to be 2 point squared.

3.1.2. Processing

For this study, we adopt the Pytorch python package [51] for our network training. We adopted 3 different configurations of batch size (32, 64, and 128) along with 2 configurations for lr (1×10^{-2} and 1×10^{-3}) and momentum (0 and 0.9) for hyperparamter tuning.

For each iteration during the training (i.e., batch), the loss is calculated from forward-propagating the training samples using the cross-entropy loss function (CEL, as defined in Equation (2)).

$$H(p, q) = -\sum_{i=1}^{n} p(x_i) \log(q(x_i)) \tag{2}$$

where n stands for number of classes (in our case $n = 2$), $p(x)$ stands for the actual distribution, and $q(x)$ stands for the predicted distribution. CEL can be used to evaluate the differences between the actual distribution and the predicted distribution. Before initiating the back-propagation process, the outputs is first adjusted by the learning rate (which is initially set to 0.001) profile. Then, during the back-propagation process, each neuron is adjusted by taking partial derivatives.

As the loss consistently decreases with each epoch iteration, the learning rates is then dynamically adjusted using the ExponentialLR learning rate scheduler in conjunction with Stochastic Gradient Descent (SGD) as the optimizer. Continuously applying the validation set during training allowed us to detect any possible issues with the model's structure or hyperparameters. For example, if the ACC of the validation set does not increase with time or the loss starts to diverge, we can simply terminate the training and adjust the parameters before the training process ends, known as early stopping.

We note that a combination of 50 epochs, a batch size of 32, a momentum of 0.9, and an lr of 1×10^{-3} yields the best performance. The bottom panel of Figure 3 shows

the validation curve for our model with optimized hyperparameters. The validation performance peaked at the 30th epoch, achieving an overall validation accuracy of ∼95%. Subsequently, the model trained at the 30th epoch is then used for all our future analyses.

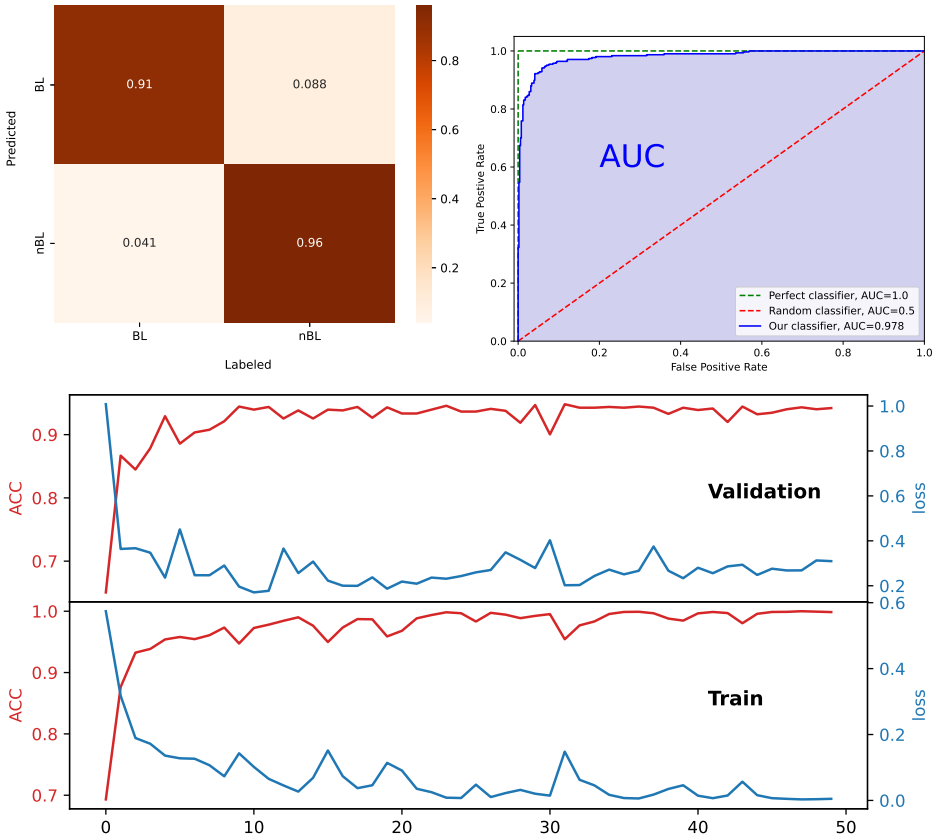

Figure 3. The testing and training results. A normalized confusion matrix for the test set (**top left**). The vertical axis (Labeled) stands for the results labeled by frequency spectra, while the horizontal axis (Predicted) stands for the results predicted by our CNN model. The receiver operating characteristic curve (ROC) and AUC for our model (**top right**), and the ROC curve and AUC for a random classifier and a perfect classifier are drawn and labeled for comparison. The area under the ROC curve for the perfect classifier (plotted in green) and the random classifier (plotted in red) is 1.0 and 0.5, respectively. The training curves are attached at the bottom.

3.1.3. Testing

After the training process, we test the performance of the model using the test set. More specifically, we first apply the model to the images of phased light curves from the test set. Then, we normalize the outputs based on the Softmax function, as given in Equation (3):

$$P_{BL} = \frac{\exp(O_{BL})}{\exp(O_{BL}) + \exp(O_{nBL})} \tag{3}$$

where P_{BL} represent the possibility of being BL stars, and O_{BL} and O_{nBL} represents the output for labels BL and nBL, respectively. Stars with P_{BL} greater than 0.5 are classified as BL candidates and vice versa. We then compare the classification results with those obtained from frequency analysis to determine the performance of the model. These results are discussed in detail in Section 4.1. A flow chart of the procedures that we used to train the model can be found in Figure 4.

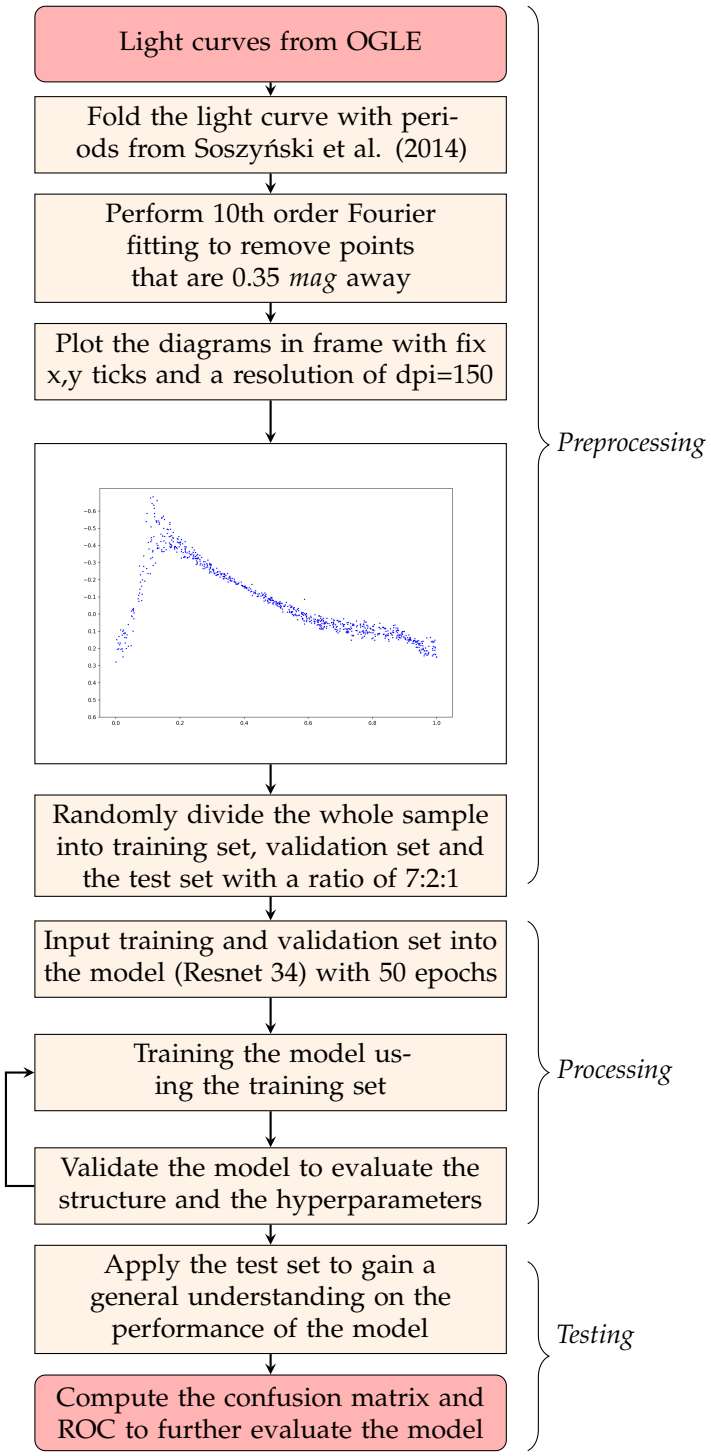

Figure 4. The training process for our model (for our entire data set). The captions on the right indicate the stage to which the training belongs (consistent with the subsections in 3.1 Network training) Soszyński et al. [6].

4. Results

4.1. The Test Set Results

The test set consists of 819 stars in total, as determined based on the 7:2:1 split performed in Section 2. Our model is then evaluated by constructing a confusion matrix using the sources in the test set. Based on the confusion matrix, we first determine that the ACC parameter for our model is 94%. Therefore, given that the results of the training process are satisfactory, we believe there is no need to adjust the hyperparameters to re-train the

model. This conclusion finds support in our training curve, presented in the lower panel of Figure 3.

Regarding the test set, we find that the estimated TNR (=0.96) is higher than or comparable to the TPR (=0.91). The phase curves of sources mislabeled by our CNN model are then examined in greater detail. A notable observation is that a significant portion of these mislabeled sources exhibit either noisy phase curves or low pulsation amplitudes (i.e., amplitude < 0.3 mag). The presence of noisy phase curves may challenge the model, as it may struggle to discern genuine BL pulsation within the noise. Additionally, given that only a minority of RRab stars demonstrate small pulsation amplitudes, it is probable that the model under-learns the differences between BL and nBL stars in these cases. Meanwhile, a very small fraction of the sources that are marked as nBL by PS17 and labeled as BL by our model exhibit clear BL modulation in their phase curves and frequency spectra. Likely, some of the sources from PS17 [26] with under-detected BL peaks were recovered with the release of more data in 2019.

We then evaluate our model based on the receiver operating curve and use it to compute the area under the curve statistic (AUC) (as given in Figure 3, top right panel). The estimated AUC for our model based on the test set is 0.98, indicating significant differences in the phased light curves for those with and without the BL effect. We apply the MLP model developed by them in P19 [48] to our samples from the test set for further comparison. The results are given in Table 1. Note that the estimated AUC and ACC parameters for the MLP model are slightly higher than those given by P19 [48]. Such differences may have originated from the random shuffle process performed during preprocessing, potentially resulting in our test set comprising distinct samples compared to those from P19 [48]. By comparing the testing results using our test set, we note that our CNN model is 10% more sensitive in detecting BL effects compared with MLP developed by P19 [48] (i.e., our TPR is 10% higher).

Table 1. A comparison of the model parameters for *test set* and MC Sample. Note that the definitions for ACC and AUC are provided in Section 3, while the definitions for TPR and TNR are given in Section 4.1.

Sample	Study	ACC	AUC	TPR	TNR
Test set	This study	0.94	0.98	0.91	0.96
-	P19 [48]	0.88	0.94	0.81	0.92
-	Frequency analysis	1.00	1.00	1.00	1.00
MC Sample	This study	0.91	0.97	0.85	0.97
-	P19 [48]	0.86	0.91	0.80	0.88
-	Frequency analysis	1.00	1.00	1.00	1.00

4.2. MC Sample

Among 290 stars in the MC Sample, 113 and 177 stars are classified as BL and nBL candidates by our CNN model, respectively. The classification results are provided in Table 2.

Then, we re-classify our MC Sample using the method suggested by PS17 [26] to further evaluate the performance of our model. Following the procedures suggested by PS17 [26], we first pre-whiten the main pulsation frequency (f_0) along with its first 10 harmonics and search for the existence of significant side peaks in the range of $f_0 \pm 0.3[c/d]$ in the residuals. Then, we classify our samples into different subgroups based on the position and amplitude of the peaks in the frequency spectra. Note that the qualities of the phased light curve from the MC Sample are not as good as those from GB Sample 1

because of fewer data points (as shown in Figure 1). Consequently, it might be difficult to determine whether these BL candidates are modulated or not when they have fewer significant side peaks (3.5 S/N) in the frequency spectra. Thus, we classify stars with fewer significant side peaks as BL candidates or cBL stars. Also, those with unresolved peaks (closer than 1.5/time span to f_0) are labeled as period changing (PC). Also, we reject some stars that showed irregular and weird modulations on the phased light curves (labeled as **Rejection**). We believe that these stars might suffer from blending effects or instrumental effects. A detailed description of the four subgroups can be found below:

1. **BL**: There is at least one resolved strong peak, with the amplitude variation having S/N above 4, observed in the range of $f_0 - 0.3[c/d]$ and $f_0 + 0.3[c/d]$;
2. **nBL**: The peak S/N is less than 3.5, observed in the range of $f_0 - 0.3[c/d]$ and $f_0 + 0.3[c/d]$;
3. **cBL & PC**: Amplitude in the range of 3.5 S/N to 4 S/N and frequency the range of $f_0 - 0.3[c/d]$ and $f_0 + 0.3[c/d]$ on the frequency spectra. Stars with peaks greater than 4 S/N but not resolved are labeled as **cBL & PC** as well;
4. **Rejection (REJ)**: Stars show uncanny modulation, likely due to their poor light-curve quality.

Table 2. The Classification results for the MC Sample. The full table is provided along with the published version[2]. A portion is shown here for guidance regarding its formatting.

OGLE ID	RA (deg)	Decl (deg)	Mean *I*-Band Magnitude	Prediction
OGLE-LMC-RRLYR-00455	70.155705	−70.050611	17.295	nBL
OGLE-LMC-RRLYR-00487	70.30854	−68.463278	16.87	nBL
OGLE-LMC-RRLYR-00732	71.202	−67.01375	17.443	nBL
OGLE-LMC-RRLYR-00733	71.206455	−67.851111	17.157	nBL
OGLE-LMC-RRLYR-00736	71.211255	−66.717361	15.765	nBL
OGLE-LMC-RRLYR-00773	71.33571	−69.834083	17.551	nBL
OGLE-LMC-RRLYR-00854	71.58459	−68.424889	13.353	BL
OGLE-LMC-RRLYR-00904	71.745255	−68.784778	14.85	nBL
OGLE-LMC-RRLYR-01047	72.14325	−70.110611	17.938	nBL
OGLE-LMC-RRLYR-01881	73.71342	−67.016972	16.506	nBL
...	...	...	...	...

Finally, we finalize the classification results by re-examining the phased light curve for the **BL** and **nBL** subgroups to check for any signs of BL modulation, so that we could avoid possible biases caused by the frequency analysis method. Meanwhile, note that a few exceptions have been made during the classification process. Stars with no obvious modulation on the phase curve but with only one significant peak (>4 S/N) around $2.005[c/d]$ on the residuals of the frequency spectra are labeled as **nBL**. These peaks can be induced by various instrumental effects according to PS17 [26]. Some examples of **cBL & PC**, **nBL**, and **Rejection** can be found in Figure 5.

In total, we find 120 **BL** samples, 137 **nBL** samples, 29 **cBL & PC** samples, and 4 **Rejection** samples from the frequency analysis. Then, we match our frequency analysis results to our CNN results to determine the confusion matrix for the MC Sample, which is found in Figure 6.

Similarly, we derive the ACC, AUC, TPR, and TNR parameters based on the confusion matrix determined based on the MC Sample, and the results are listed in Table 1. For comparison, we also apply the MLP developed by P19 [48] to the MC Sample to obtain the above parameters. We provide these results in Table 1 as well.

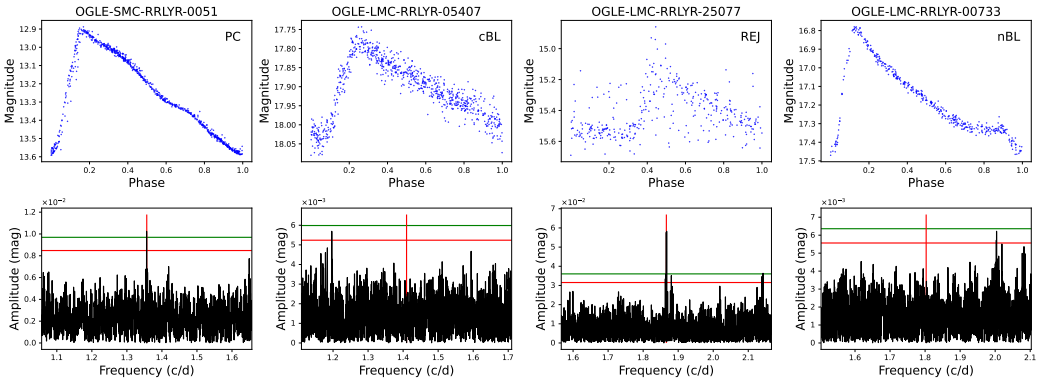

Figure 5. Phased light curves and frequency spectra for different classes that have been newly introduced, including unresolved peak (**cBL & PC**), a peak greater than 3.5 S/N but smaller than 4 S/N (**cBL**), **REJ**, peaks around 2.005$[c/d]$ (**nBL**), from left to right. The red and green horizontal lines indicate 3.5 S/N and 4 S/N, respectively. Also, the red vertical line stands for f_0. Note that the frequency spectra included in the bottom row have been pre-whitened already. We excluded sources (e.g., 25,077) with poor light-curve quality from our analysis. The significant peak near 2.005 [c/d] in 00733's frequency spectra is likely due to instrumental effects (see text); therefore, we label it as an nBL star.

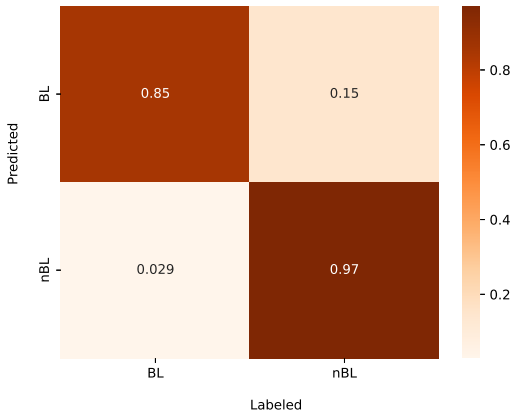

Figure 6. A normalized confusion matrix for the MC Sample. The vertical axis (Labeled) stands for the results labeled by frequency spectra, while the horizontal axis (Predicted) stands for the results predicted by our CNN model.

We note that all the parameters estimated from the MC Sample are lower than those from the test set. We believe it is likely that the light curves of the sources that we included in the test set have much better light-curve quality and sampling compared with those from the MC Sample, as expected from Section 2.

These misclassified samples are subsequently subjected to careful examination as well. Similar to the test set, these inaccurately classified test samples exhibit lower amplitudes or noisier light curves in comparison to those classified correctly.

We also note that the BL stars from LMC and SMC have also been well-studied by the Massive Compact Halo Object (MACHO) project [19]. The MACHO sample contains 6391 RR Lyrae stars, and 731 of them are identified as BL stars. Among the 23 stars that we have in common, we recovered all the BL stars discovered by MACHO.

4.3. GB Sample 2

The classification result for our GB Sample 2 are provided in Table 3.

Table 3. The classification results for the GB Sample 2. The full table is provided, along with the published version See note 2 above. A portion is shown here for guidance regarding its formatting.

OGLE ID	RA (deg)	Decl (deg)	Mean *I*-Band Magnitude	Prediction
OGLE-BLG-RRLYR-00247	258.668625	−29.492833	15.846	nBL
OGLE-BLG-RRLYR-00253	258.69825	−29.442611	15.392	nBL
OGLE-BLG-RRLYR-00270	258.77592	−29.347194	16.666	BL
OGLE-BLG-RRLYR-00366	260.87466	−29.063778	16.683	BL
OGLE-BLG-RRLYR-00369	260.889585	−29.289778	16.16	nBL
OGLE-BLG-RRLYR-00372	260.899335	−29.370972	16.064	BL
OGLE-BLG-RRLYR-00375	260.90967	−29.4155	17.153	BL
OGLE-BLG-RRLYR-00376	260.91063	−29.203694	16.682	nBL
OGLE-BLG-RRLYR-00377	260.914455	−29.290694	16.292	nBL
OGLE-BLG-RRLYR-00381	260.92584	−29.247722	16.498	BL
...	...	...	...	...

For sources that we included in GB Sample 2, 2496 of them are classified as BL candidates by our CNN, with a rate of 31%. We notice that this rate is lower than that found by PS17 [26] using GB samples from the OGLE-IV survey (i.e., 40%). One of the possible explanations is that GB Sample 2 has fewer points per light curve in comparison with GB Sample 1. When the light curve is relatively poorly sampled, the BL modulations are more likely to be covered by noise. The possible impact of the sampling of the light curve is discussed further in Section 5. It is worth noting that the incidence rate of the modulated stars from OGLE observations is much lower than that from the Kepler K2 mission [52], who have suggested that the occurrence rate of BL modulation can reach up to ∼90%, perhaps due to their higher-quality light curves obtained from the *Kepler* mission. The occurrence rate of the BL effect using light curves obtained from ground-based observations seems to range from 10% to 60%. Previous studies indicate that the rate of BL stars seems to be extremely high in the galactic field, in a range from 31% [25] to 60% [53]. The rates found from the M3 and Galactic Gulge are about 50% [30] and 40.3% PS17 [26], respectively. Their estimated rates are derived from the data taken by a Schmidt telescope from the Konkoly Observatory and OGLE-IV survey, respectively. The fraction of BL stars is found to be 37% in NGC6362 [35] and 69% in NGC5024 [54], respectively. In comparison, the LMC tends to show an extremely low rate of BL stars, with a fraction of only 10% [19,55]. For the SMC, the BL fraction is about 20% [56,57]. The lower fraction of BL stars in LMC and SMC is perhaps related to their relatively low-quality light curves. See Kovacs [17] for a summary of the occurrence rate in different environments. It is also worth mentioning that a portion of stars from our GB Sample 2 could be misclassified by our CNN, resulting in a relatively high or low occurrence rate. Similarly, we found that roughly 16% of the stars from GB Sample 2 are classified differently by our CNN compared with their MLP.

Considering that the characteristics of BL stars in the GB region were previously well-studied by PS17 [26], we thus compare the distribution of various light-curve parameters for labeled BL and nBL samples between GB Samples 1 & 2. Regarding the GB Sample 2 data set, we make use of the classification result determined from both the MLP model developed by P19 [48] and the ones determined by our CNN model for comparison.

4.3.1. Period–Amplitude Relations

Figure 7 presents the period and amplitude distributions of BL/nBL stars categorized by our CNN method and P19 [48]. We then apply a Kolmogorov–Smirnov test (KS-test) to further examine if they follow the same distribution. We denote the following:

- $p_{1,C}$: the *p*-value of the KS-test of GB Sample 1 and GB Sample 2 using the CNN's classification result;
- $p_{C,M}$: KS-test *p*-value between the CNN and MLP classification results on GB Sample 2.

For this, we compare the period and amplitude distributions classified based on our CNN to the ones discovered by P19 [48] and PS17 [26] for BL and nBL sources separately. Quite surprisingly, we determined, for both BL and nBL sources, classifications using CNN and frequency analysis could yield similar amplitude distributions (i.e., $p_{1,C} > 0.999$). We observe a similar resemblance for the distribution of period for BL/nBL samples classified by CNN and MLP as well (i.e., $p_{C,M} > 0.999$).

However, from Figure 7, we note that there are ∼5% BL stars (∼10% nBL stars) with an amplitude of less than 0.2 mag in GB Sample 2. Based on our CNN's classification, the differences in distribution between these low-amplitude BL and nBL samples are similar to those with higher amplitudes. However, as discussed in [7], those samples with smaller amplitudes might suffer from blending effects.

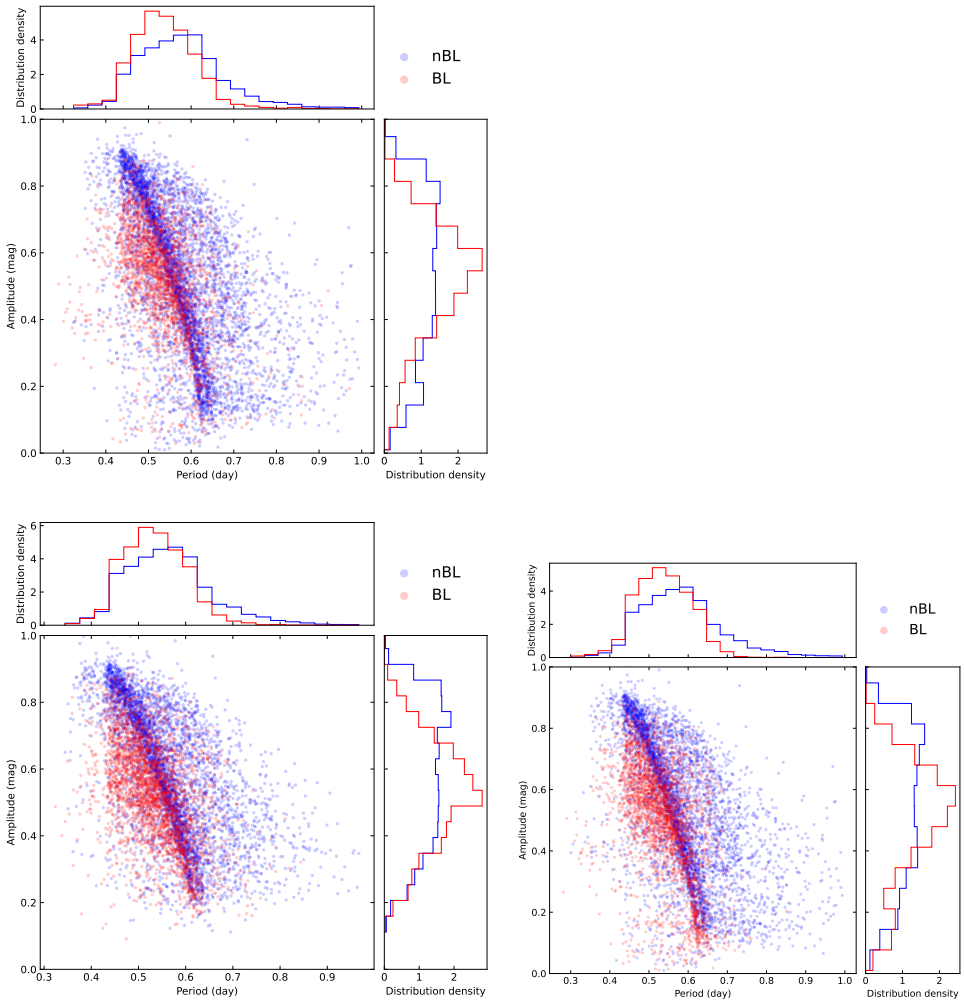

Figure 7. A comparison between the distribution of BL/nBL stars on the Bailey diagram based on various classification methods. **Top**: GB Sample 2 classified by our CNN model. **Bottom left**: GB Sample 1 classified based on frequency analysis techniques. **Bottom right**: GB Sample 2 classified by the MLP developed by P19 [48]. Note that density stands for the distribution after normalization.

4.3.2. Fourier Parameters

We then make use of Fourier parameters to further characterize the differences between our GB Sample 1 and GB Sample 2. Fourier parameters R_{21} and R_{31} stand for amplitude ratios between the 2nd and 1st components and 3rd and 1st, respectively. Meanwhile, ϕ_{21} and ϕ_{31} denote the phase differences between the 2nd and 1st and the 3rd and 1st components, respectively. The Fourier parameters for GB Sample 1 and GB Sample 2 are taken from Soszyński et al. [6] and Soszyński et al. [7], respectively. Calculations of these parameters are based on Equation (4),

$$m(t) = A_0 + \sum_{i=1}^{n} A_i \cos\left(2\pi i \frac{(t - t_0)}{P} + \phi_i\right) \tag{4}$$

where ϕ_i and A_i represent phase and amplitude, respectively, and n is the degree of the fit, while P stands for the pulsation period. Simon and Lee [58] define the relevant parameters as $R_{i1} = \frac{A_i}{A_1}$ and $\phi_{i1} = \phi_i - i\phi_1$.

We present the distribution of R_{21}, R_{31} and ϕ_{21}, ϕ_{31} for GB Sample 1 from PS17 [26] and GB Sample 2 in Figures 8 and 9, respectively. For GB Sample 2, nBL stars tend to have slightly higher R_{21}, R_{31}, consistent with the trend seen in GB Sample 1 PS17 [26]. Figures 8 and 9 reveal that the distributions of BL and nBL stars in the Fourier parameter space using our CNN classification algorithm are similar for GB Sample 1 and GB Sample 2.

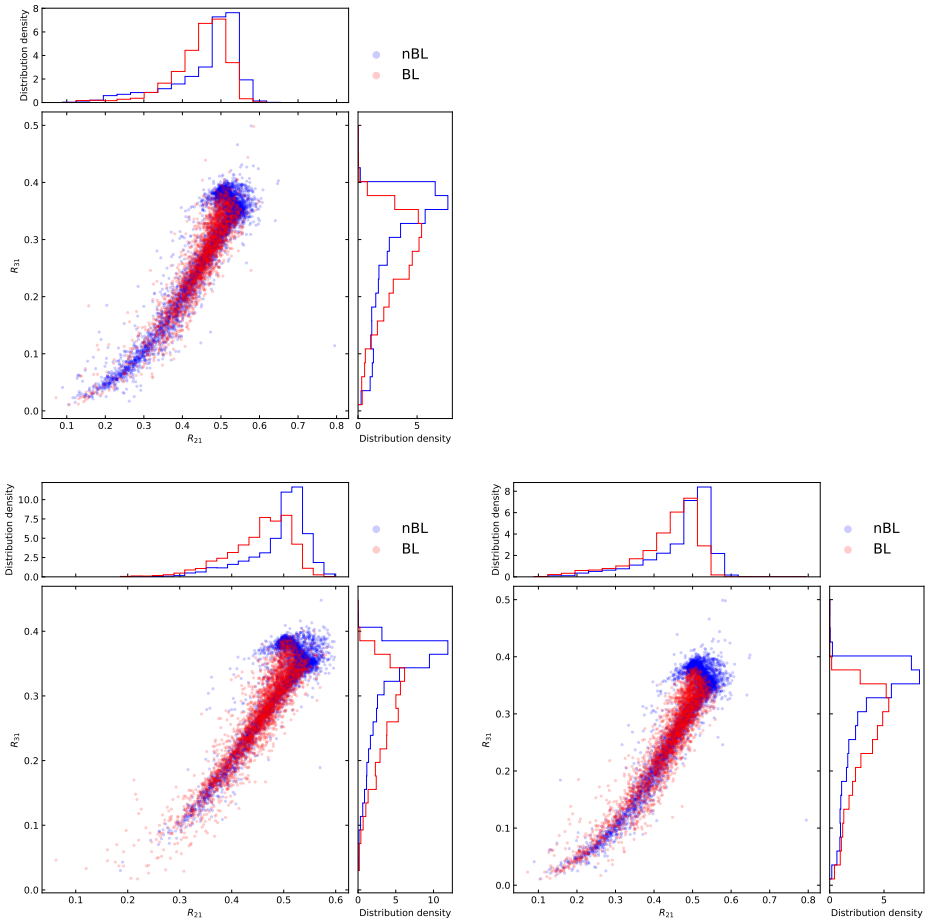

Figure 8. A comparison between the distribution of BL/nBL stars on $R_{21} - R_{31}$ diagram based on various classification techniques. **Top**: GB Sample 2 classified by our CNN model. **Bottom left**: GB Sample 1 classified based on frequency analysis technique. **Bottom right**: GB Sample 2 classified by the MLP method developed by P19 [48]. Note that the density stands for the distribution after normalization.

We then apply a KS-test to test the resemblance between the distribution of Fourier parameters using labeling results from different techniques. We find that the values of $p_{1,C}$ derived for BL and nBL subsamples are both greater than 0.999 for all Fourier parameters, indicating that classifications using CNN and frequency analysis yield similar distributions of Fourier parameters. Such a trend is also found for both BL and nBL subclasses labeled by the CNN and MLP techniques ($p_{C,M} > 0.999$). Following P19 [48], we examine the R_{31}–ϕ_{31} distribution for GB Sample 2 and MC Sample as well. We present the results in Figure 10.

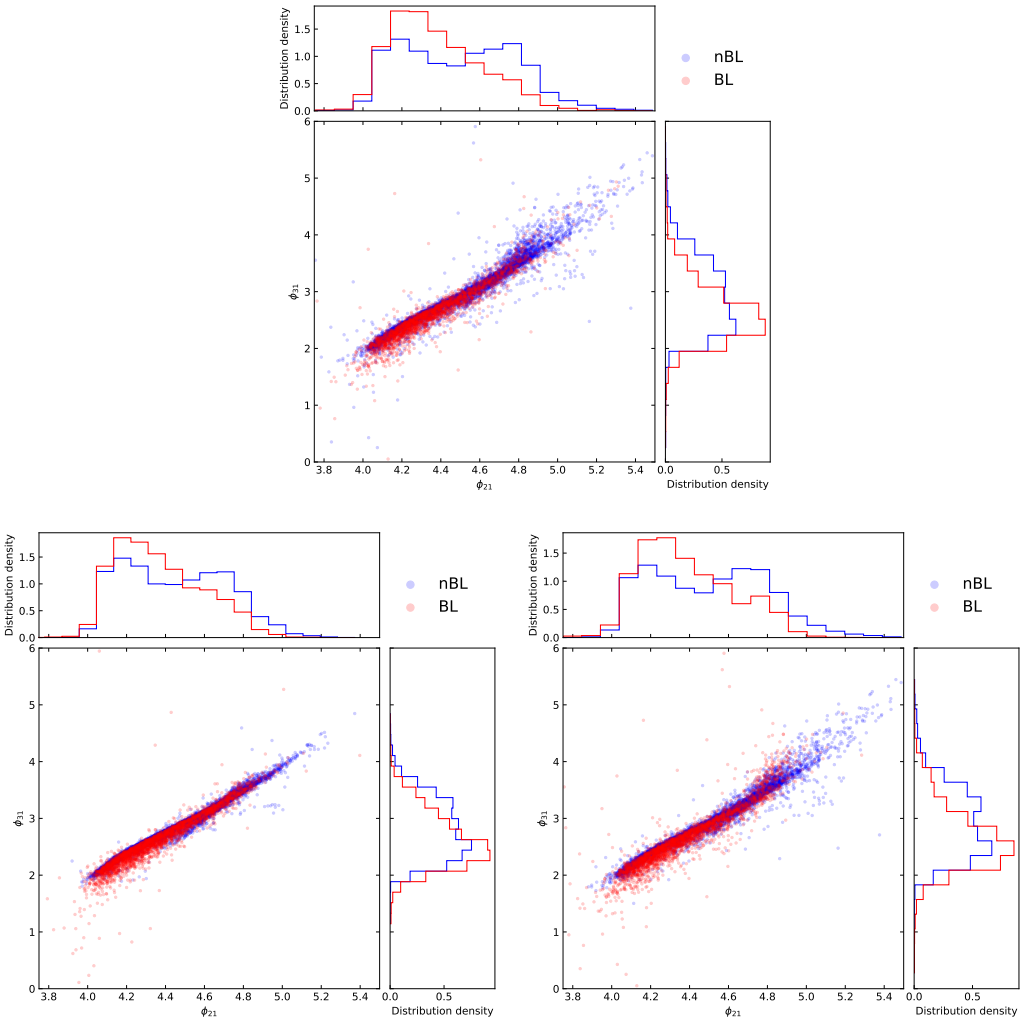

Figure 9. A comparison between the distribution of BL/nBL stars on $\phi_{21} - \phi_{31}$ diagram from various classification techniques. **Top**: GB Sample 2 classified by our CNN model. **Bottom left**: GB Sample 1 classified based on frequency analysis techniques. **Bottom right**: GB Sample 2 classified by the MLP method developed by P19 [48]. Note that the density stands for the distribution after normalization.

It is noteworthy that the hook structure observed among the nBL samples from P19 [48] has also been observed in GB Sample 2 and MC Sample. These findings from light-curve characteristics directly suggested that our CNN-based classifications for GB Sample 2 are reliable and can be used well in future studies.

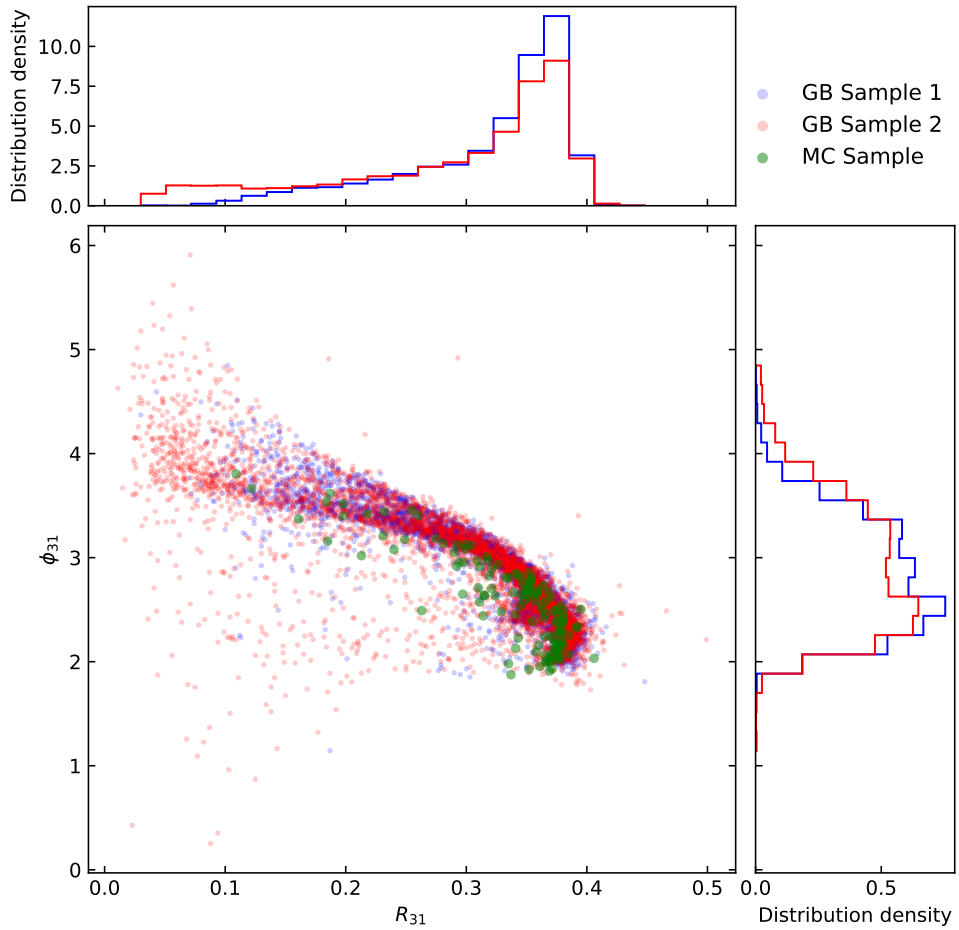

Figure 10. A comparison between the distribution of nBL stars on R_{31}–ϕ_{31} diagram from GB Sample 1 (classified from frequency analysis), GB Sample 2 (classified by our CNN), and MC Sample (classified by our CNN). Note that density stands for the distribution after normalization.

5. Discussion

Our analysis from the test set, GB Sample 2, and the MC Sample confirm that the CNN method can identify the BL subclass from RRab samples effectively. Therefore, we believe that our model can be used well in identifying the BL candidates from a large amount of RRab light curves. In comparison with the traditionally used frequency analysis method and the MLP method developed by P19 [48], our CNN method can be more reliable (e.g., with up to 10% increase in sensitivity) and efficient when dealing with larger data sets.

On the other hand, our results from Section 4 suggested that the identification quality for the MC Sample is lower than the test set. Thus, we further discuss the possible reasons that might lead to this difference.

Firstly, we examine the distribution of light-curve parameters between correctly and incorrectly classified samples for GB Sample 2 and the MC Sample. Meanwhile, we cross-match our BL samples from the test set with those from Skarka et al. [59] to obtain an estimate of the Blazhko frequencies and study its impact on our classification quality.

We find no significant differences between subsamples labeled incorrectly and those labeled correctly based on Figure 11. However, for the incorrectly classified sample, we find an outlier peak at the higher end of the Period$_{BL}$ distribution. We note that the peak is caused by only two stars, which could be due to the effect of a small number of statistics. On the other hand, it could be the case that, since Period$_{BL}$ is longer, the light curve covers

fewer BL cycles within its coverage period and, therefore, Period_{BL} is less significant in the frequency space and is, hence, harder to identify.

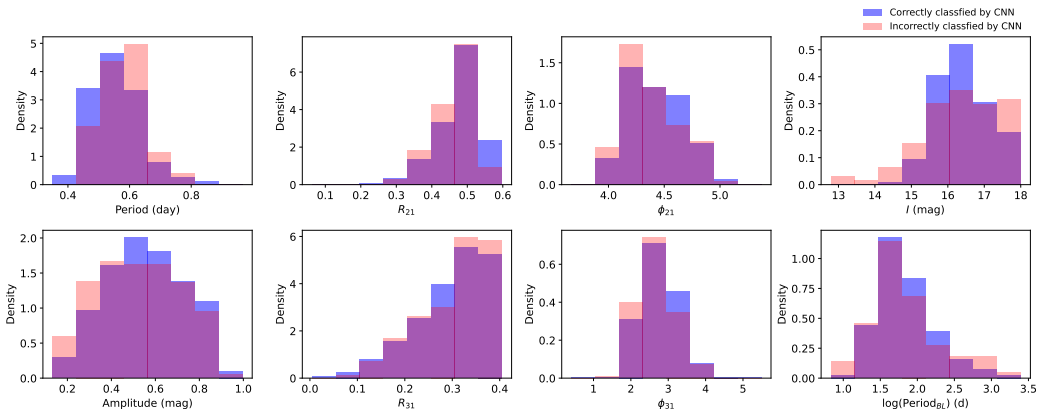

Figure 11. A comparison between the distribution of samples classified correctly and incorrectly by our CNN method. Note that the density stands for the distribution after normalization. Note that the Period_{BL} is taken from Skarka et al. [59]

Then, we calculate a Spearman correlation coefficient with its associated p-value between the P_{BL} from Equation (3) and light-curve parameters, including period, amplitude, Fourier parameters, number of data points, and median magnitude error for each light curve. The Spearman correlation coefficient (R_s) is calculated as follows:

$$R_s = \frac{\mathrm{cov}(\mathrm{R}(X), \mathrm{R}(Y))}{\sigma_{\mathrm{R}(X)}\sigma_{\mathrm{R}(Y)}} \tag{5}$$

where $\mathrm{R}(X_i), \mathrm{R}(Y_i)$ are the rank variables of the associated variables X_i and Y_i, $\mathrm{cov}(\mathrm{R}(X), \mathrm{R}(Y))$ is the co-variance of the rank variables, and $\sigma_{\mathrm{R}(X)}$ and $\sigma_{\mathrm{R}(Y)}$ are the standard deviations for the rank variables. The results of the calculations are shown in Figure 12.

An analysis of Figure 12 reveals that the Spearman correlation coefficient p derived for the MC Sample is much larger than those derived for the other two data sets, perhaps due to limited sample size. The p-values of all the parameters derived on the base of the test set and GB Sample 2 are smaller than 0.01, while the typical p-value is greater than 0.1 for the MC Sample.

It is noteworthy that the P_{BL} parameter seems to have moderately negative dependence on R_{21} and R_{31} for all of the three data sets, indicating that the nBL sample tends to have larger R_{21} and R_{31} values. This is consistent with the trends shown in Figure 8. Both Jurcsik [60] and PS17 [26] observed similar trends using samples from Messier 3 (M3), Galactic Disk, and Galactic Bulge.

We observe some weak impact of amplitude on our results for GB Sample 2 but not for the MC Sample and the test set. We believe that this weak negative correlation might be a consequence of the blended stars, as discussed in Section 4.3.1. We also observed some weak correlations between P_{BL} and ϕ_{31} for GB Sample 2 and the test set, while no notable trend has been observed for the MC Sample.

We also notice that the number of epochs for each light curve is negatively correlated with P_{BL} for the MC Sample. This indicates that, in the MC Sample, the stars that have been classified as nBL tend to have more points per light curve than those identified as BL stars. Note, however, that we have not observed such a trend in GB Sample 2 and the test set. The reason for this might be that GB Sample 2 and the test set have more data points per light curve, so such a correlation is not apparent. Meanwhile, the correlation between the number of epochs per light curve and P_{BL} for the MC Sample has an extremely high p-

value for the correlation test (i.e., 0.37), indicating that this result might not be generalizable to other data sets. On the other hand, we observe an opposite trend in the test set. This perhaps reflects the fact that BL stars with more epochs per light curve can be detected more easily. Similar trends have also been observed by PS17 [26]. Figure 3 suggested that stars with fewer data points tend to have higher noise levels in the frequency spectra.

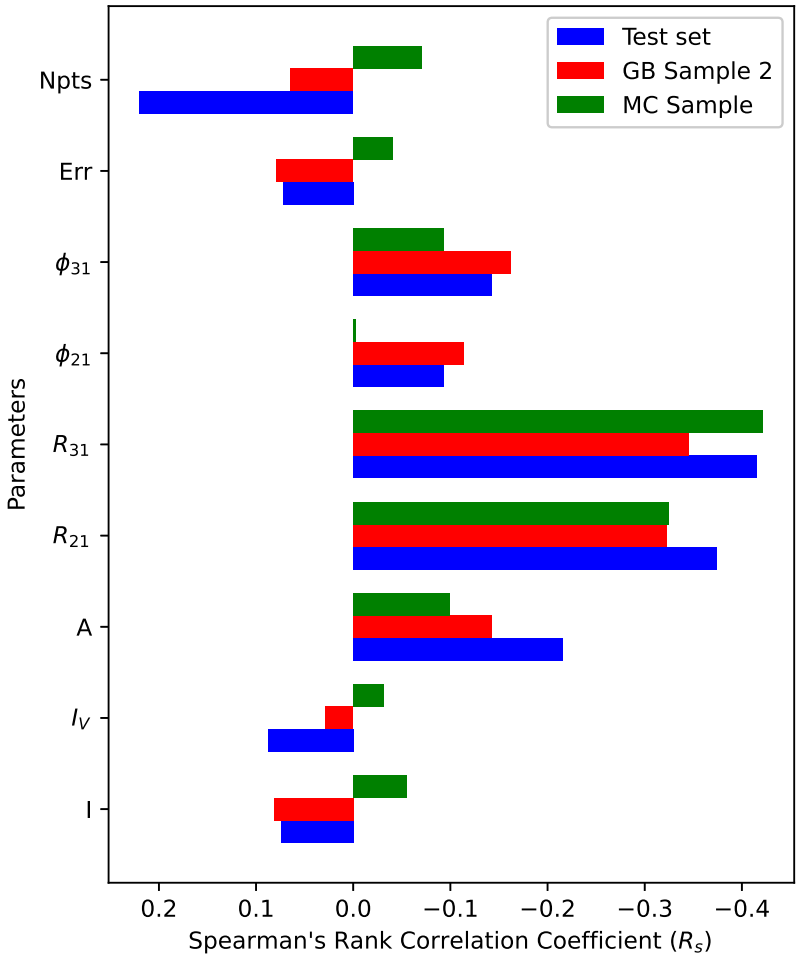

Figure 12. Spearman correlation coefficient derived for each parameter that we investigated. The parameters are labeled on the *y*-axis, while the values on the *x*-axis represent the associated Spearman correlation coefficients.

However, the disparity between the MC Sample and the test set, particularly in terms of the P_{BL}–number of epochs correlation, which suggests a potentially weaker performance of the model on data sets with fewer epochs per light curve. This discrepancy may be attributed to overfitting, where the model is trained predominantly on light curves with more epochs compared to those present in the MC Sample. To further understand how the number of epochs could impact the performance of our model, we examine how accuracy (ACC) varies with changes in the number of epochs for all our test samples together (i.e., MC sample + test set). More specifically, we partition the epochs into multiple bins and calculate the ACC within each bin using data from the test/validation set and the MC sample. Inspecting Figure 13, we observe a decrease in performance when we decrease the number of epochs, from a typical test set accuracy (95%) to typical ACCs from the MC Sample (91%). The bins exhibiting lower performance predominantly originated from the MC Sample, hence offering a plausible explanation for the decline in performance within

the MC sample. This observed decline in performance could potentially limit our model's ability to detect BL effects from samples with inferior light-curve quality.

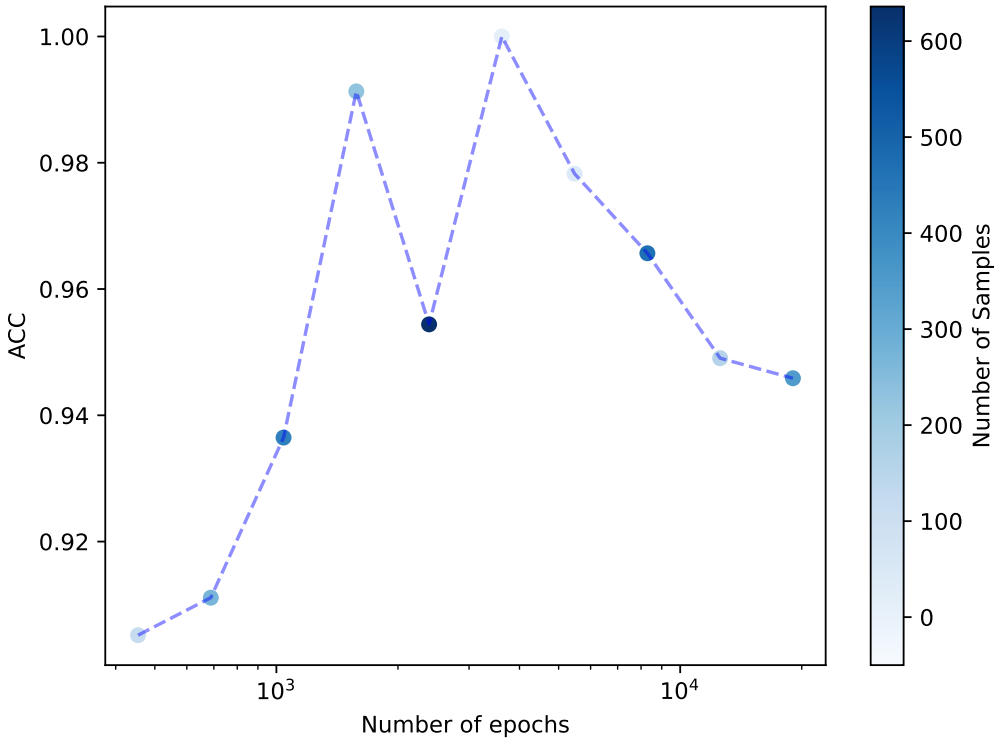

Figure 13. Number of epochs vs. ACC for our test samples. Please note that the transparency of the dots has been adjusted to correspond with the number of samples contained within each bin.

Consequently, one potential approach to enhance the model's performance is to incorporate more light curves with marginal BL modulations, corresponding to marginal BL peaks in the frequency spectra. Nonetheless, such an augmentation must be approached with caution, as many of these marginal BL cases might not truly be BL at all (refer to PS17 [26]), potentially leading to further confusion within the model. It is worth noting that, despite the diminished performance observed in our most degenerate test samples, primarily from the MC sample, the ACC remains superior to the model constructed by PS19, underscoring the robustness of our network architecture.

On the other hand, based on the source-by-source analysis, we note that the model seems to struggle to classify sources with low amplitudes. These low-amplitude sources may be under-represented in the data set, given that RRab stars typically exhibit higher amplitudes. Therefore, as an improvement to this model, future studies could introduce more low-amplitude sources in the data set for training to reinforce the existence of these low-amplitude sources.

Notably, no significant correlation has been observed between P_{BL} and other light-curve parameters, such as ϕ_{31}, ϕ_{21}, mean I-band magnitude, and error, for each light curve in both the MC Sample and GB Sample 2. These findings suggest that the introduced cut-offs for mean magnitude, error, and number of data points may reduce the risk of overfitting the model.

While we acknowledge that these cut-offs may introduce additional bias to our testing results. For example, despite the observation that sources from the MC Sample tend to have degenerate light curves compared to the other two data sets, these sources still pass many of the cut-offs that we set to ensure reasonable data quality for identification. As a result, the testing results derived based on these sources might be biased towards the better

end. Furthermore, the plotting process may introduce additional biases into the training procedure. Factors such as image resolution and the size of the plotted points can influence how the data are visually represented. However, as shown in Figure 2, the current plotting configuration still allows for a clear distinction between BL and nBL stars.

Recursive neural networks (RNNs) present a potential avenue for improving our classification model even further. RNNs have demonstrated comparable or superior performance to CNNs in handling time-series data and have been effectively applied to variable star classification (e.g., [61]). However, incorporating RNNs would require additional modifications to our data set, which we defer to future studies.

The >8000 more newly classified RRab stars across two different sky regions allow us to provide insights into the physical origin of the Blazhko effect at a statistical significance level. Hence, in the next series of papers, we aim to use statistical analysis combined with the power of machine learning to answer questions, such as, Is there a physical difference between BL and nBL stars? If so, which one differs by the most? Which light-curve parameter can best represent the modulation induced by the BL effect? These questions will be addressed in a forthcoming paper.

6. Summary

In this study, we develop a new method to identify the RRab samples with the Blazhko effect. The identification model is built based on the classic CNN model, ResNet 34, without any modifications to its original structure.

After dividing BL/nBL sources classified by frequency spectra from GB Sample 1 into the training set, validation set, and test set with a ratio of 7:2:1, the model is trained to identify BL stars. This training process involved using the training set with the help of the validation set directly from diagrams of the phased light curves to train our CNN model. Using the test set, we estimate that our model has an ACC of 0.935 and an AUC of 0.978. As the pulsation period for each source is not taken into account in our training process, the high ACC and AUC scores for our model further indicate that the BL modulation can be well-characterized by light-curve structure without considering the period of pulsation.

We then apply our model to 290 stars from the MC Sample to present a further evaluation of our identification model. After applying frequency analysis to the MC Sample to obtain the true labels, we labeled 118 samples as BL and 137 samples as nBL based on the criteria that we suggested in Section 4.2. Based on a crossmatch between the results from frequency analysis and our CNN's classification, we conclude that our model has ACC and AUC values of 0.90 and 0.95, respectively, for the MC Sample. We believe that the model parameters estimated from the MC Sample are lower compared with those estimated from the test set. The Spearman analysis indicates that the difference in light-curve quality between GB Samples 1 and 2 might be responsible for the differences in model parameters.

Compared with traditionally used frequency analysis methods, our method can be more efficient and faster in identifying RRab stars with the Blazhko effect from huge data sets. More importantly, our model can understand the light-curve characteristics of both BL and nBL objects better than the existing machine learning methods such as MLP, with up to 10% more sensitivity in identifying BL stars. Additionally, we note that our CNN's identification quality could also be impacted by the sampling of the light curve. However, its overall dependence on light-curve quality is comparable with those required by frequency analysis according to our evaluation. We did not find significant differences between correctly and incorrectly labeled samples for all the light-curve parameters that we studied. Therefore, we believe that our model can be applied well in future large-variability searches, to identify the BL stars faster and more accurately.

We then apply our CNN model to the newly selected GB Sample 2. In total, we identified 2615 BL candidates, with a rate of 32% out of 8123 stars from GB Sample 2. We then apply a KS-test to GB Sample 1 and CNN-labeled GB Sample 2. This revealed that, among all the light-curve characteristics that we discussed (period, amplitude, and Fourier parameters), the distribution of BL and nBL samples from GB Sample 2 based on our CNN labels matches that of GB Sample 1 with $p > 0.999$. Additionally, the differences between BL and nBL samples of GB Sample 2 based on our CNN's classification mostly resemble those found for GB Sample 1 for both samples with both higher (i.e., $A > 0.2$) and lower (i.e., $A \leq 0.2$) amplitudes. However, we also noticed that our samples have comparably smaller amplitudes relative to stars from GB Sample 1. This might be an indication that some ($\sim$10%) of our samples from GB Sample 2 suffer from the blending effect. Such an amplitude-related bending effect has also been suggested by using the Spearman test. In the future, these newly discovered BL candidates will be used to present a detailed analysis of the light curve and physical differences between BL and nBL stars.

Author Contributions: N.J. wrote the paper and performed the analysis under the guidance of X.W., B.S., and L.W. T.S. and S.P. helped train the CNN model. X.L. helped with the manuscript. All authors have read and agreed to the published version of the manuscript.

Funding: This work is supported by the National Science Foundation of China (NSFC grants 12288102, 12033003, and 11633002) and the Tencent Xplorer Prize. L.W. is sponsored (in part) by the Chinese Academy of Sciences (CAS), through a grant to the CAS South America Center for Astronomy (CASSACA) in Santiago, Chile.

Data Availability Statement: Data will be shared upon request to the corresponding author.

Acknowledgments: We thank the referee for providing constructive comments. We acknowledge the comments from Christopher D. Matzner and the support of Period04 by Patrick Lenz. We are also very grateful for the helpful comments from Zdeněk Prudil.

Conflicts of Interest: The authors declare no conflicts of interest.

Note

[1] Cycle per day.
[2] https://drive.google.com/drive/folders/1T9aeGOQCmBjrZzmVM5J1e2qd1n-si1gr?usp=sharing

References

1. Catelan, M.; Smith, H.A. *Pulsating Stars*; Wiley-VCH: Weinheim, Germany, 2015.
2. Samus', N.N.; Kazarovets, E.V.; Durlevich, O.V.; Kireeva, N.N.; Pastukhova, E.N. General catalogue of variable stars: Version GCVS 5.1. *Astron. Rep.* **2017**, *61*, 80–88. [CrossRef]
3. Oliveira, R.A.P.; Ortolani, S.; Barbuy, B.; Kerber, L.O.; Maia, F.F.S.; Bica, E.; Cassisi, S.; Souza, S.O.; Pérez-Villegas, A. Precise distances from OGLE-IV member RR Lyrae stars in six bulge globular clusters. *Astron. Astrophys.* **2022**, *657*, A123. [CrossRef]
4. Prudil, Z.; Hanke, M.; Lemasle, B.; Crestani, J.; Braga, V.F.; Fabrizio, M.; Koch-Hansen, A.J.; Bono, G.; Grebel, E.K.; Matsunaga, N.; et al. Milky Way archaeology using RR Lyrae and type II Cepheids. I. The Orphan stream in 7D using RR Lyrae stars. *Astron. Astrophys.* **2021**, *648*, A78. [CrossRef]
5. Minniti, D. et al. [The MACHO Collaboration]. RR Lyrae Stars in the MACHO Database. *arXiv* **1996**, arXiv:astro-ph/9610025. [CrossRef]
6. Soszyński, I.; Udalski, A.; Szymański, M.K.; Pietrukowicz, P.; Mróz, P.; Skowron, J.; Kozłowski, S.; Poleski, R.; Skowron, D.; Pietrzyński, G.; et al. Over 38000 RR Lyrae Stars in the OGLE Galactic Bulge Fields. *Acta Astron.* **2014**, *64*, 177–196. [CrossRef]
7. Soszyński, I.; Udalski, A.; Szymański, M.K.; Wyrzykowski, Ł.; Ulaczyk, K.; Poleski, R.; Pietrukowicz, P.; Kozłowski, S.; Skowron, D.M.; Skowron, J.; et al. The OGLE Collection of Variable Stars. Over 45 000 RR Lyrae Stars in the Magellanic System. *Acta Astron.* **2016**, *66*, 131–147. [CrossRef]
8. Soszyński, I.; Udalski, A.; Wrona, M.; Szymański, M.K.; Pietrukowicz, P.; Skowron, J.; Skowron, D.; Poleski, R.; Kozłowski, S.; Mróz, P.; et al. Over 78 000 RR Lyrae Stars in the Galactic Bulge and Disk from the OGLE Survey. *Acta Astron.* **2019**, *69*, 321–337. [CrossRef]

9. Drake, A.J.; Djorgovski, S.G.; Mahabal, A.; Beshore, E.; Larson, S.; Graham, M.J.; Williams, R.; Christensen, E.; Catelan, M.; Boattini, A.; et al. First Results from the Catalina Real-Time Transient Survey. *Astrophys. J.* **2009**, *696*, 870–884. [CrossRef]
10. Pojmanski, G. The All Sky Automated Survey. Catalog of Variable Stars. I. 0 h - 6 h Quarter of the Southern Hemisphere. *Acta Astron.* **2002**, *52*, 397–427. [CrossRef]
11. Chambers, K.C.; Magnier, E.A.; Metcalfe, N.; Flewelling, H.A.; Huber, M.E.; Waters, C.Z.; Denneau, L.; Draper, P.W.; Farrow, D.; Finkbeiner, D.P.; et al. The Pan-STARRS1 Surveys. *arXiv* **2016**, arXiv:1612.05560. [CrossRef]
12. Sesar, B.; Stuart, J.S.; Ivezić, Ž.; Morgan, D.P.; Becker, A.C.; Woźniak, P. Exploring the Variable Sky with LINEAR. I. Photometric Recalibration with the Sloan Digital Sky Survey. *Astron. J.* **2011**, *142*, 190. [CrossRef]
13. Clementini, G.; Ripepi, V.; Garofalo, A.; Molinaro, R.; Muraveva, T.; Leccia, S.; Rimoldini, L.; Holl, B.; Jevardat de Fombelle, G.; Sartoretti, P.; et al. Gaia Data Release 3. Specific processing and validation of all-sky RR Lyrae and Cepheid stars: The RR Lyrae sample. *Astron. Astrophys.* **2023**, *674*, A18. [CrossRef]
14. Hernitschek, N.; Stassun, K.G. The Impact of Observing Strategy on the Reliable Classification of Standard Candle Stars: Detection of Amplitude, Period, and Phase Modulation (Blazhko Effect) of RR Lyrae Stars with LSST. *Astrophys. J.* **2022**, *258*, 4. [CrossRef]
15. Blažko, S. Mitteilung über veränderliche Sterne. *Astron. Nachrichten* **1907**, *175*, 325. [CrossRef]
16. Buchler, J.R.; Kolláth, Z. On the Blazhko Effect in RR Lyrae Stars. *Astrophys. J.* **2011**, *731*, 24. [CrossRef]
17. Kovacs, G. The Blazhko phenomenon. *Commmunications Konkoly Obs. Hung.* **2016**, *105*, 61–68. [CrossRef]
18. Sódor, Á.; Jurcsik, J.; Molnár, L.; Szeidl, B.; Hurta, Z.; Bakos, G.Á.; Hartman, J.; Béky, B.; Noyes, R.W.; Sasselov, D.; et al. First Results of the Konkoly Blazhko Survey II. In *Proceedings of the Progress in Solar/Stellar Physics with Helio- and Asteroseismology*; Shibahashi, H., Takata, M., Lynas-Gray, A.E., Eds.; Astronomical Society of the Pacific Conference Series; Astronomical Society of the Pacific: Hakone, Japan, 2012; Volume 462, p. 228. [CrossRef]
19. Alcock, C.; Alves, D.R.; Becker, A.; Bennett, D.; Cook, K.H.; Drake, A.; Freeman, K.; Geha, M.; Griest, K.; Kovacs, G.; et al. The macho project large magellanic cloud variable star inventory. Xi. Frequency analysis of the fundamental-mode rr lyrae stars. *Astrophys. J.* **2003**, *598*, 597–609. [CrossRef]
20. Benkő, J.M.; Plachy, E.; Szabó, R.; Molnár, L.; Kolláth, Z. Long-timescale Behavior of the Blazhko Effect from Rectified Kepler Data. *Astrophys. J.* **2014**, *213*, 31. [CrossRef]
21. Szabó, R.; Kolláth, Z.; Molnár, L.; Kolenberg, K.; Kurtz, D.W.; Bryson, S.T.; Benkő, J.M.; Christensen-Dalsgaard, J.; Kjeldsen, H.; Borucki, W.J.; et al. Does Kepler unveil the mystery of the Blazhko effect? First detection of period doubling in Kepler Blazhko RR Lyrae stars. *Mon. Not. R. Astron. Soc.* **2010**, *409*, 1244–1252. [CrossRef]
22. Plachy, E.; Benkő, J.M.; Kolláth, Z.; Molnár, L.; Szabó, R. Non-linear dynamical analysis of the Blazhko effect with the Kepler space telescope: The case of V783 Cyg. *Mon. Not. R. Astron. Soc.* **2014**, *445*, 2810–2817. [CrossRef]
23. Benkő, J.M.; Kolenberg, K.; Szabó, R.; Kurtz, D.W.; Bryson, S.; Bregman, J.; Still, M.; Smolec, R.; Nuspl, J.; Nemec, J.M.; et al. Flavours of variability: 29 RR Lyrae stars observed with Kepler. *Mon. Not. R. Astron. Soc.* **2010**, *409*, 1585–1593. [CrossRef]
24. Le Borgne, J.F.; Klotz, A.; Poretti, E.; Boër, M.; Butterworth, N.; Dumont, M.; Dvorak, S.; Hambsch, F.J.; Hund, F.; Kugel, F.; et al. The All-sky GEOS RR Lyr Survey with the TAROT Telescopes: Analysis of the Blazhko Effect. *Astron. J.* **2012**, *144*, 39. [CrossRef]
25. Skarka, M. Bright Blazhko RRab Lyrae stars observed by ASAS and the SuperWASP surveys. *Astron. Astrophys.* **2014**, *562*, A90. [CrossRef]
26. Prudil, Z.; Skarka, M. Blazhko effect in the Galactic bulge fundamental mode RR Lyrae stars—I. Incidence rate and differences between modulated and non-modulated stars. *Mon. Not. R. Astron. Soc.* **2017**, *466*, 2602–2613. [CrossRef]
27. Skarka, M.; Liška, J.; Auer, R.F.; Prudil, Z.; Juráňová, A.; Sódor, Á. The SERMON project: 48 new field Blazhko stars and an investigation of modulation-period distribution. *Astron. Astrophys.* **2016**, *592*, A144. [CrossRef]
28. Gillet, D. Atmospheric dynamics in RR Lyrae stars. The Blazhko effect. *Astron. Astrophys.* **2013**, *554*, A46. [CrossRef]
29. Gillet, D.; Fokin, A.B. Emission lines and shock waves in RR Lyrae stars. *Astron. Astrophys.* **2014**, *565*, A73. [CrossRef]
30. Jurcsik, J.; Smitola, P.; Hajdu, G.; Nuspl, J. On the Modulation of RR Lyrae Stars in the Globular Cluster M3. *Astrophys. J.* **2014**, *797*, L3. [CrossRef]
31. Jurcsik, J.; Hajdu, G.; Dékány, I.; Nuspl, J.; Catelan, M.; Grebel, E.K. Blazhko modulation in the infrared. *Mon. Not. R. Astron. Soc.* **2018**, *475*, 4208–4222. [CrossRef]
32. Kolláth, Z. Some Notes on the Modelling of Blazhko Effect. In *Proceedings of the RR Lyrae 2017 Conference. Revival of the Classical Pulsators: From Galactic Structure to Stellar Interior Diagnostics, Niepolomice Royal Castle*; Polskie Towarzystwo Astronomiczne: Niepolomice, Poland, 2018; Proceedings of the Polish Astronomical Society; Volume 6, pp. 137–145.
33. Skarka, M. Known Galactic field Blazhko stars. *Astron. Astrophys.* **2013**, *549*, A101. [CrossRef]
34. Benkő, J.M.; Szabó, R.; Paparó, M. Blazhko RR Lyrae light curves as modulated signals. *Mon. Not. R. Astron. Soc.* **2011**, *417*, 974–991. [CrossRef]
35. Smolec, R.; Moskalik, P.; Kałużny, J.; Pych, W.; Różyczka, M.; Thompson, I.B. RR Lyrae stars in NGC 6362. *Mon. Not. R. Astron. Soc.* **2017**, *467*, 2349–2366. [CrossRef]

36. Alzubaidi, L.; Zhang, J.; Humaidi, A.J.; Al-Dujaili, A.; Duan, Y.; Al-Shamma, O.; Santamaría, J.; Fadhel, M.A.; Al-Amidie, M.; Farhan, L. Review of deep learning: Concepts, CNN architectures, challenges, applications, future directions. *J. Big Data* **2021**, *8*, 53. [CrossRef] [PubMed]
37. Sharma, K.; Kembhavi, A.; Kembhavi, A.; Sivarani, T.; Abraham, S.; Vaghmare, K. Application of convolutional neural networks for stellar spectral classification. *Mon. Not. R. Astron. Soc.* **2020**, *491*, 2280–2300. [CrossRef]
38. Sun, Z.; Bobra, M.G.; Wang, X.; Wang, Y.; Sun, H.; Gombosi, T.; Chen, Y.; Hero, A. Predicting Solar Flares Using CNN and LSTM on Two Solar Cycles of Active Region Data. *Astrophys. J.* **2022**, *931*, 163. [CrossRef]
39. Mahabal, A.; Sheth, K.; Gieseke, F.; Pai, A.; Djorgovski, S.G.; Drake, A.J.; Graham, M.J. Deep-learnt classification of light curves. In Proceedings of the 2017 IEEE Symposium Series on Computational Intelligence (SSCI), Honolulu, HI, USA, 27 November–1 December 2017; pp. 1–8. [CrossRef]
40. Teachey, A.; Kipping, D. Identifying potential exomoon signals with convolutional neural networks. *Mon. Not. R. Astron. Soc.* **2021**, *508*, 2620–2633. [CrossRef]
41. Davies, A.; Serjeant, S.; Bromley, J.M. Using convolutional neural networks to identify gravitational lenses in astronomical images. *Mon. Not. R. Astron. Soc.* **2019**, *487*, 5263–5271. [CrossRef]
42. Yu, L.; Vanderburg, A.; Huang, C.; Shallue, C.J.; Crossfield, I.J.M.; Gaudi, B.S.; Daylan, T.; Dattilo, A.; Armstrong, D.J.; Ricker, G.R.; et al. Identifying Exoplanets with Deep Learning. III. Automated Triage and Vetting of TESS Candidates. *Astron. J.* **2019**, *158*, 25. [CrossRef]
43. Dattilo, A.; Vanderburg, A.; Shallue, C.J.; Mayo, A.W.; Berlind, P.; Bieryla, A.; Calkins, M.L.; Esquerdo, G.A.; Everett, M.E.; Howell, S.B.; et al. Identifying Exoplanets with Deep Learning. II. Two New Super-Earths Uncovered by a Neural Network in K2 Data. *Astron. J.* **2019**, *157*, 169. [CrossRef]
44. Szklenár, T.; Bódi, A.; Tarczay-Nehéz, D.; Vida, K.; Marton, G.; Mező, G.; Forró, A.; Szabó, R. Image-based Classification of Variable Stars: First Results from Optical Gravitational Lensing Experiment Data. *Astrophys. J. Lett.* **2020**, *897*, L12. [CrossRef]
45. Szklenár, T.; Bódi, A.; Tarczay-Nehéz, D.; Vida, K.; Mező, G.; Szabó, R. Variable Star Classification with a Multiple-input Neural Network. *Astrophys. J.* **2022**, *938*, 37. [CrossRef]
46. Jacyszyn-Dobrzeniecka, A. M. and Skowron, D. M. and Mróz, P. and Soszyński, I. and Udalski, A. and Pietrukowicz, P. and Skowron, J. and Poleski, R. and Kozłowski, S. and Wyrzykowski, Ł. and Pawlak, M. and Szymański, M. K. and Ulaczyk, K. OGLE-ing the Magellanic System: Three-Dimensional Structure of the Clouds and the Bridge using RR Lyrae Stars. *Acta Astronomica* **2017**, *67*, 1–35.
47. Lenz, P.; Breger, M. Period04: A software package to extract multiple frequencies from real data. *Proc. Int. Astron. Union* **2004**, *2004*, 786–790. [CrossRef]
48. Prudil, Z.; Dékány, I.; Catelan, M.; Smolec, R.; Grebel, E.K.; Skarka, M. On the Oosterhoff dichotomy in the Galactic bulge: I. Spatial distribution. *Mon. Not. R. Astron. Soc.* **2019**, *484*, 4833–4848. [CrossRef]
49. Basodi, S.; Ji, C.; Zhang, H.; Pan, Y. Gradient amplification: An efficient way to train deep neural networks. *Big Data Min. Anal.* **2020**, *3*, 196–207. [CrossRef]
50. He, K.; Zhang, X.; Ren, S.; Sun, J. Deep Residual Learning for Image Recognition. *arXiv* **2015**, arXiv:1512.03385. [CrossRef]
51. Paszke, A.; Gross, S.; Massa, F.; Lerer, A.; Bradbury, J.; Chanan, G.; Killeen, T.; Lin, Z.; Gimelshein, N.; Antiga, L.; et al. PyTorch: An Imperative Style, High-Performance Deep Learning Library. *arXiv* **2019**, arXiv:1912.01703. [CrossRef]
52. Kovacs, G. On the Incidence Rate of Blazhko Stars. *arXiv* **2020**, arXiv:2004.06452. [CrossRef]
53. Szabó, R.; Benkő, J.M.; Paparó, M.; Chapellier, E.; Poretti, E.; Baglin, A.; Weiss, W.W.; Kolenberg, K.; Guggenberger, E.; Le Borgne, J.F. Revisiting CoRoT RR Lyrae stars: Detection of period doubling and temporal variation of additional frequencies. *Astron. Astrophys.* **2014**, *570*, A100. [CrossRef]
54. Arellano Ferro, A.; Bramich, D.M.; Figuera Jaimes, R.; Giridhar, S.; Kuppuswamy, K. The unusually large population of Blazhko variables in the globular cluster NGC 5024 (M53)*: Blazhko variables in NGC 5024. *Mon. Not. R. Astron. Soc.* **2012**, *420*, 1333–1346. [CrossRef]
55. Chen, B.Q.; Jiang, B.W.; Yang, M. Analysis of a selected sample of RR Lyrae stars in the LMC from OGLE-III. *Res. Astron. Astrophys.* **2013**, *13*, 290–312. [CrossRef]
56. Soszyński, I.; Udalski, A.; Szymański, M.K.; Kubiak, M.; Pietrzyński, G.; Wyrzykowski, Ł.; Szewczyk, O.; Ulaczyk, K.; Poleski, R. The Optical Gravitational Lensing Experiment. The OGLE-III Catalog of Variable Stars. III. RR Lyrae Stars in the Large Magellanic Cloud. *Acta Astron.* **2009**, *59*, 1–18. [CrossRef]
57. Soszyński, I.; Udalski, A.; Szymański, M.K.; Kubiak, J.; Pietrzyński, G.; Wyrzykowski, Ł.; Ulaczyk, K.; Poleski, R. The Optical Gravitational Lensing Experiment. The OGLE-III Catalog of Variable Stars. IX. RR Lyr Stars in the Small Magellanic Cloud. *Acta Astron.* **2010**, *60*, 165–178. [CrossRef]
58. Simon, N.R.; Lee, A.S. The structural properties of cepheid light curves. *Astrophys. J.* **1981**, *248*, 291–297. [CrossRef]
59. Skarka, M.; Prudil, Z.; Jurcsik, J. Blazhko effect in the Galactic bulge fundamental mode RR Lyrae stars—II. Modulation shapes, amplitudes, and periods. *Mon. Not. R. Astron. Soc.* **2020**, *494*, 1237–1249. [CrossRef]

60. Jurcsik, J. Blazhko-type fundamental-mode RR Lyrae stars in the globular cluster M3. *Mon. Not. R. Astron. Soc.* **2019**, *490*, 80–95. [CrossRef]
61. Naul, B.; Bloom, J.S.; Pérez, F.; van der Walt, S. A recurrent neural network for classification of unevenly sampled variable stars. *Nat. Astron.* **2018**, *2*, 151–155. [CrossRef]